Measurement of the complex transmittance of large optical elements with Ptychographical Iterative Engine

Hai-Yan Wang,[1] Cheng Liu,[1,*] Suhas P Veetil,[2] Xing-Chen Pan,[1] and Jian-Qiang Zhu[1]

[1]*Shanghai Institute of Optics and Fine Mechanics, Chinese Academy of Sciences, Shanghai 201800, China*
[2]*Department of Physics, Amity University Dubai, Dubai 345019, United Arab Emirates*
[*]*cheng.liu@hotmail.co.uk*

Abstract: Wavefront control is a significant parameter in inertial confinement fusion (ICF). The complex transmittance of large optical elements which are often used in ICF is obtained by computing the phase difference of the illuminating and transmitting fields using Ptychographical Iterative Engine (PIE). This can accurately and effectively measure the transmittance of large optical elements with irregular surface profiles, which are otherwise not measurable using commonly used interferometric techniques due to a lack of standard reference plate. Experiments are done with a Continue Phase Plate (CPP) to illustrate the feasibility of this method.

References and links

1. D. J. Trummer, R. J. Foley, and G. S. Shaw, "Stability of optical elements in the NIF target area building," in *Third International Conference on Solid State Lasers for Application to Inertial Confinement Fusion* (International Society for Optics and Photonics, 1999), 363–371.
2. W. H. Williams, J. M. Auerbach, M. A. Henesian, J. K. Lawson, J. T. Hunt, R. A. Sacks, and C. C. Widmayer, "Modeling characterization of the National Ignition Facility focal spot," in *Optoelectronics and High-Power Lasers and Applications* (International Society for Optics and Photonics, 1998), pp. 93–104.
3. J. Lindl, "Development of the indirect-drive approach to inertial confinement fusion and the target physics basis for ignition and gain," Phys. Plasmas **2**(11), 3933–4024 (1995).
4. D. Malacara, *Optical Shop Testing* (John Wiley, 2007),Chap. 15.
5. W. Jiang and H. Li, "Hartmann-Shack wavefront sensing and wavefront control algorithm," in *The Hague'90, 12–16 April* (International Society for Optics and Photonics, 1990), 82–93.
6. G. Cao and X. Yu, "Accuracy analysis of a Hartmann-Shack wavefront sensor operated with a faint object," Opt. Eng. **33**(7), 2331–2335 (1994).
7. V. Y. Zavalova and A. V. Kudryashov, "Shack-Hartmann wavefront sensor for laser beam analyses," in *International Symposium on Optical Science and Technology* (International Society for Optics and Photonics, 2002), 277–284.
8. S. Sato, T. Mori, Y. Higashi, S. Haya, M. Otsuka, and H. Yamamoto, "A profilometer for synchrotron radiation mirrors," J. Electron Spectrosc. Relat. Phenom. **80**, 481–484 (1996).
9. X. Liu, Y. Gao, and M. Chang, "A partial differential equation algorithm for wavefront reconstruction in lateral shearing interferometry," J. Opt. A Pure Appl. Opt. **11**(4), 045702 (2009).
10. R. Gerchberg, "A practical algorithm for the determination of phase from image and diffraction plane pictures," Optik **35**, 237–246 (1972).
11. J. R. Fienup, "Reconstruction of an object from the modulus of its Fourier transform," Opt. Lett. **3**(1), 27–29 (1978).
12. J. Fienup, "Space object imaging through the turbulent atmosphere," Opt. Eng. **18**(5), 529–534 (1979).
13. J. Fienup, "Iterative method applied to image reconstruction and to computer-generated holograms," Opt. Eng. **19**(3), 297–305 (1980).
14. J. M. Rodenburg and H. M. Faulkner, "A phase retrieval algorithm for shifting illumination," Appl. Phys. Lett. **85**(20), 4795–4797 (2004).
15. S. Matsuoka and K. Yamakawa, "Wave-front measurements of terawatt-class ultrashort laser pulses by the Fresnel phase-retrieval method," J. Opt. Soc. Am. B **17**(4), 663–667 (2000).
16. G. R. Brady and J. R. Fienup, "Measurement of an optical surface using phase retrieval," in *Optical Fabrication and Testing* (Optical Society of America, 2006).

17. S.-W. Bahk, J. Bromage, J. D. Zuegel, and J. R. Fienup, "Application of Phase Retrieval for Predicting a High-Intensity Focused Laser Field," in *Conference on Lasers and Electro-Optics* (Optical Society of America, 2008).
18. G. R. Brady, M. Guizar-Sicairos, and J. R. Fienup, "Optical wavefront measurement using phase retrieval with transverse translation diversity," Opt. Express **17**(2), 624–639 (2009).
19. A. M. Maiden, J. M. Rodenburg, and M. J. Humphry, "Optical ptychography: a practical implementation with useful resolution," Opt. Lett. **35**(15), 2585–2587 (2010).
20. C. Liu, T. Walther, and J. M. Rodenburg, "Influence of thick crystal effects on ptychographic image reconstruction with moveable illumination," Ultramicroscopy **109**(10), 1263–1275 (2009).
21. X. Pan, C. Liu, Q. Lin, and J. Zhu, "Ptycholographic iterative engine with self-positioned scanning illumination," Opt. Express **21**(5), 6162–6168 (2013).
22. C. A. Haynam, P. J. Wegner, J. M. Auerbach, M. W. Bowers, S. N. Dixit, G. V. Erbert, G. M. Heestand, M. A. Henesian, M. R. Hermann, K. S. Jancaitis, K. R. Manes, C. D. Marshall, N. C. Mehta, J. Menapace, E. Moses, J. R. Murray, M. C. Nostrand, C. D. Orth, R. Patterson, R. A. Sacks, M. J. Shaw, M. Spaeth, S. B. Sutton, W. H. Williams, C. C. Widmayer, R. K. White, S. T. Yang, and B. M. Van Wonterghem, "National Ignition Facility laser performance status," Appl. Opt. **46**(16), 3276–3303 (2007).
23. J. Néauport, X. Ribeyre, J. Daurios, D. Valla, M. Lavergne, V. Beau, and L. Videau, "Design and optical characterization of a large continuous phase plate for Laser Integration Line and laser Megajoule facilities," Appl. Opt. **42**(13), 2377–2382 (2003).

1. Introduction

High-power solid state laser facilities employed in inertial confinement fusion (ICF) make use of several large optical components and wavefront control systems to ensure that high energy laser pulses are delivered with the required spot size and energy density [1]. The transmittance of these large optical components determines the quality of the laser pulses generated and the final performance of the whole facility. Any inaccuracies in material uniformity or surface profile of such optical systems would obviously distort the spatial and temporal shape of the pulses and, in some cases, cause catastrophic damage to the entire high-power laser system [2,3]. Thus a strict quality control of the wavefront is an important task for researches in ICF. In principle, all phase-measurement techniques including interferometry, holography, and surface-profile metrology [4] can be employed to measure the complex transmittance of these optical components. However, these techniques are not ideal to evaluate the performance of large apertures. For example, with a Shack-Hartmann wavefront sensor [5,6], which is widely used for the wavefront detection, the transmittance function of an optical element can be measured easily by passing parallel light beam through it and thus detecting the phase of the transmitted field [7]. However, its resolution is limited by its sub-aperture and the number of the micro-lenses, and the highest resolution reachable is D/N, where the D is the diameter of the elements and the N is the number of the micro-lenses of the sensor along a given direction. Most of the optical elements used in our ICF systems have a diameter of about 40cm, and with a Shack-Hartmann sensor of 200×200 micro-lenses the spatial resolution is only about 2mm. Another device that can be used to measure the optical transmittance is the interferometer, such as Fizeau interferometer and Twyman-Green interferometer. The advantage of interferometer lies on its high measurement accuracy, a limit of $\lambda/1000$ (in theory) in the axial direction. However, the interferometry needs a standard plate to do such a measurement, and for large aperture elements, the manufacturing of the standard plate is very difficult [8]. Shearing interferometer does not need a reference beam and a standard plate, but it can only provide a differential data of the measured wavefront. In addition, complex image processing and cumbersome algorithms are needed to reconstruct the wavefront [9]. At the same time, since only low frequency information is detected in this case depending on the shearing amount, shearing interferometer shows only an approximate shape of the wavefront.

Compared to traditional techniques used in the optical metrology, Coherent Diffractive Imaging (CDI), which can retrieve the complex phase directly from the diffraction pattern intensity seems to be a good choice for the phase measurement in the field of high intensity lasers since it is done without using any reference beam, standard plate, or imaging devices. CDI algorithm was first proposed by Gerchberg R.W. and Saxton W.O [10]. in 1971 and then

developed by Fienup [11–13]. A Ptychographical Iterative Engine (PIE) algorithm was proposed in the year 2000 by Prof. Rodenburg of Sheffield University, which reconstructs the amplitude and phase of the object from a sequence of diffraction patterns obtained by shifting the object to different distances relative to the illumination known priori to overcome the disadvantages of traditional CDI algorithms including the stagnation, low convergence, and limited view field [14]. CDI was developed mainly for the imaging with short wavelength radiation including x-ray and electron beam, where high quality devices are not available. Owing to its simplicity in its setup and its speed in detection, traditional CDI method was also successfully used for measurements in the field of high energy laser. This include measurement of wavefront of 100-fs high energy laser pulses with a peak-valley error smaller than 0.36λ [15], surface profile of a concave spherical mirror [16] and the wave front of a chirped-pulse-amplification laser pulse [17]. Gregory R. Brady measured the transmitted wavefront of a plano-convex singlet using using phase retrieval with transverse translation diversity and the results of measurements were repeatable to within approximately 0.01λRMS [18]. In this paper we will demonstrate that PIE technique can be used to measure the complex transmittance of large aperture elements of ICF system, which cannot be accurately measured with other existing techniques.

2. Basic principle of ePIE algorithm

While the standard PIE algorithm can only measure the transmission function of the scanning object, an extended PIE (ePIE) algorithm can bring out the accurate model of the illumination function and specimen function simultaneously [19–21]. Since the illumination field also can be measured accurately, ePIE algorithm may find lots of applications in the field of the high power laser.

The details of the ePIE algorithm can be found elsewhere, and it is only briefly outlined here. The setup used for the ePIE algorithm is schematically shown in Fig. 1, where the specimen with a complex transmittance of $O(r)$ is mounted on a translation stage and is illuminated by a probe with distribution of $P(r)$, where r is the coordinate of the object plane. During the scanning of the specimen, the CCD camera in the far field records a set of diffractions $I_i(u)$, where u is the reciprocal coordinate of the direct space coordinate r. The relationship between the exit wave and the illumination probe is $\varphi(r,R)=P(r)\cdot O(r-R)$, where R is the shift of the probe to the object.
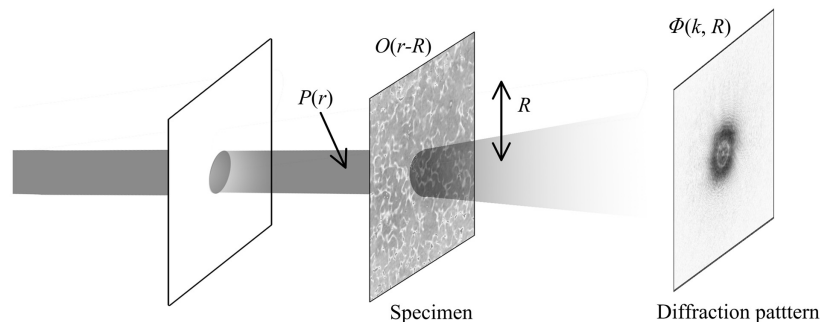

Fig. 1. Schematic of standard PIE method. The specimen is illuminated by a probe beam and the diffraction patterns are recorded in the far field.

Like the other CDI techniques, PIE makes the reconstruction iteratively by forward propagating and backward propagating the wave between the object and the detector planes.

After the diffraction patterns are recorded during the scanning of the object relative of the illumination, the reconstruction can start with random guesses for the transmission function $O(r)$ and probe $P(r)$ using the following the procedure:

(1) The exit wave function at the current position R_i is calculated with two random guesses to $P_{n,g}(r)$ and $O_{n,g}(r-R_i)$

$$\varphi_{n,g}(r,R_i)=P_{n,g}(r)\cdot O_{n,g}(r-R_i) \tag{1}$$

the subscript g, n represents a guessed function at the nth iteration.

(2) Corresponding wave function in the diffraction space plane is calculated from the Fourier transform of $\Psi_{n,g}(r,R_i)$:

$$\phi_{g,n}(k,R_i)=FFT\left[\varphi_{g,n}(r,R_i)\right]=\left|\phi_{g,n}(k,R_i)\right|e^{i\theta_n(k,R_i)} \tag{2}$$

where FFT represents the Fourier transform.

(3) The amplitude of $\phi_{n,g}(k,R_i)$ is replaced by the measured values:

$$\phi_{c,n}(k,R_i)=\sqrt{I_n}e^{i\theta_n(k,R_i)} \tag{3}$$

Where I_n is the intensity of diffraction patterns recorded by CCD, and the subscript c represents the corrected wave function.

(4) Update the guess at the exit field by inverse Fourier transform:

$$\varphi_{c,n}(r,R_i)=FFT^{-1}\left[\phi_{c,n}(k,R_i)\right] \tag{4}$$

where FFT^{-1} represents the inverse Fourier transform.

(5) Update the function $P(r)$ and $O(r-R_i)$ with the following formulas

$$O_{new}(r,R_i)=O_{g,n}(r,R_i)+\frac{|P_n(r)|}{|P_n(r)|_{max}}\frac{P_n^*(r)}{\left[|P_n(r)|^2+\alpha\right]}\left[\varphi_{c,n}(r,R_i)-P_n(r)\cdot O(r,R_i)\right] \tag{5}$$

$$P_{new}(r)=P(r)+\frac{|O(r,R_i)|}{|O(r,R_i)|_{max}}\frac{O^*(r,R_i)}{\left[|O(r,R_i)|^2+\alpha\right]}\times\left[\varphi_{c,n}(r,R_i)-P_n(r)\cdot O(r,R_i)\right] \tag{6}$$

where α is an appropriately chosen constant to suppress the noise.

(6) Repeat steps 1-5 till satisfying images are generated.

In most applications of ePIE, the scanning object with a distribution of $O(r)$ is the specimen to be measured, and the measurement of the probe $P(r)$ is done to improve the measurement accuracy. However, we use this technique here to measure the distribution of illumination $P(r)$.

3. Complex transmittance of large optical elements with ePIE

The experimental setup for measuring the transmittance of a large aperture optical element with ePIE algorithm is schematically shown in Fig. 2, where a parallel beam of 28cm in diameter is focused firstly by anon-spherical lens with a focal length of 1575mm and is then illuminated on a scanning object $O(x, y)$ near the focal plane. The object $O(x, y)$ taken is a random phase plate. The diffraction patterns are recorded by a CCD camera behind the object during the transverse scanning of the object relative to the optical axis. With the ePIE

algorithm, the illumination $P_0(x, y)$ on the object plane can be measured accurately. Then, the optical element to be measured is placed behind the condenser lens, and the illuminating field on the scanning object plane $P_1(x, y)$ can also be measured with ePIE algorithm. By propagating both $P_0(x, y)$ and $P_1(x, y)$ to a plane exactly behind the condenser lens with Fresnel diffraction formula, we can obtain the field $U(x, y)$ illuminating the optical element being studied and the field $T(x, y)$ which is leaving the optical element, respectively. The complex transmittance of the optical element studied can be obtained by calculating the phase of $U(x, y)T^*(x, y)$, where the star indicates the conjugate. The wavelength of the laser source used is 632.8nm, and the CCD used is PIKE-421B (AVT). The optical element to be studied is a Continuous Phase Plate (CPP), which has a highly irregular surface profile and is used as a key element of ICF system to smooth the laser beam of ICF system to ensure an ideal focal spot [22,23]. A small departure in its surface profile from its designed shape can drastically increase the electrical field in some place and increase the risk of radiation damage in frequency doubling crystal, focus lens, and sample grating, etc.
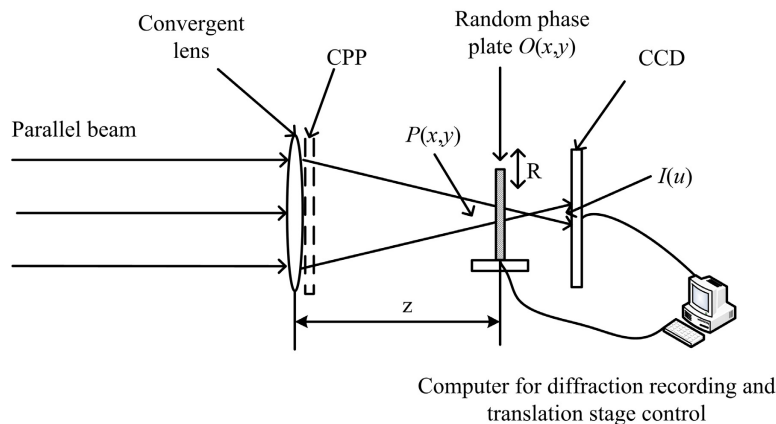

Fig. 2. Experimental setup for measuring the transmission functions with ePIE. A parallel beam focused by a non-spherical lens illuminates an object O(x, y) near the focal plane and the diffraction patterns are recorded by CCD behind the object during the transverse scanning of the object.

Figure 3(a) shows the manufactured CPP plate, where the diameter is about 31cm. Figure 3(b) is the design value of the surface profile, which can generate the required focal spot. We can find that surface profile of the CPP is highly irregular with the peak and valley heights of about 13.8714 rad and −15.4880 rad for He-Ne laser, respectively. Though the requirement on the manufacturing of the CPP is strictly high, due to its highly irregular surface profile and the large aperture, the commonly used technique cannot be used for its transmittance measurement. Figure 3(c) is the measurement result of a Zygo interferometer, where the black areas mean invalid measurement. The slope of the surface profile is too steep at these black areas, and the interference fringes are too dense to resolve. This is the reason for the existence of these immeasurable areas. Figure 3(c) is the unwrapped phase distribution with the least square method, and since this kind of phase unwrapping method is essentially a global optimization technique, the existence of the invalid measurement influences the value of the other areas, and then, the unwrapped phase in Fig. 3(c) shows no similarity to the real surface profile of CPP.
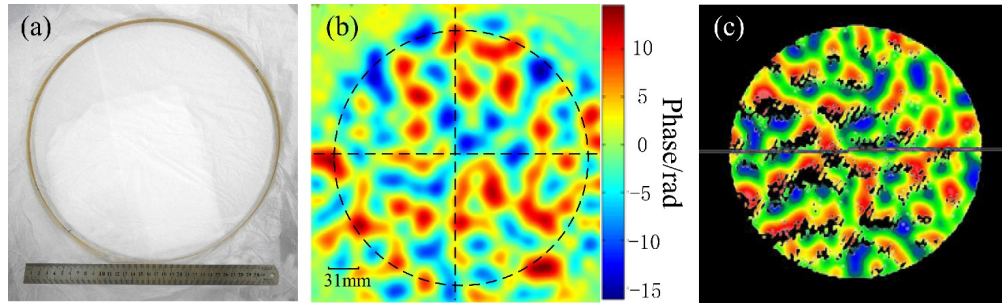
Fig. 3. (a) The CPP used in the experiment. The diameter is 31 cm, shown by the adjacent scale, (b) the designed phase distribution of CPP, and (c) the measurement of CPP by Zygo interferometer

With the experiment setup shown in Fig. 2, the diffraction patterns are recorded during the cross scanning of the object before the CPP is placed into the optical path. One of these diffraction patterns is shown in Fig. 4(a), where the obvious speckle is due to the random structure of the scanning object. With ePIE algorithm, the illumination $P(r)$ on the scanning object plane is reconstructed. Figures 4(b) and 4(c) show the reconstructed modulus and phase respectively. By propagating this numerically reconstructed field to the plane exactly behind the condenser lens, the modulus and the phase of the illuminating field $U(x, y)$ is generated. Figures 4(d) and 4(e) show the modulus and the phase of $U(x, y)$ respectively. Since the light beam at the back surface of the lens is much curved, the wrapped phase quickly oscillates along the direction of the lens radius. For clarity, only the central part of the measured phase is shown in Figs. 4(c) and 4(e), where the small circles are only displaying Moiré pattern rather than the under sampled effects.
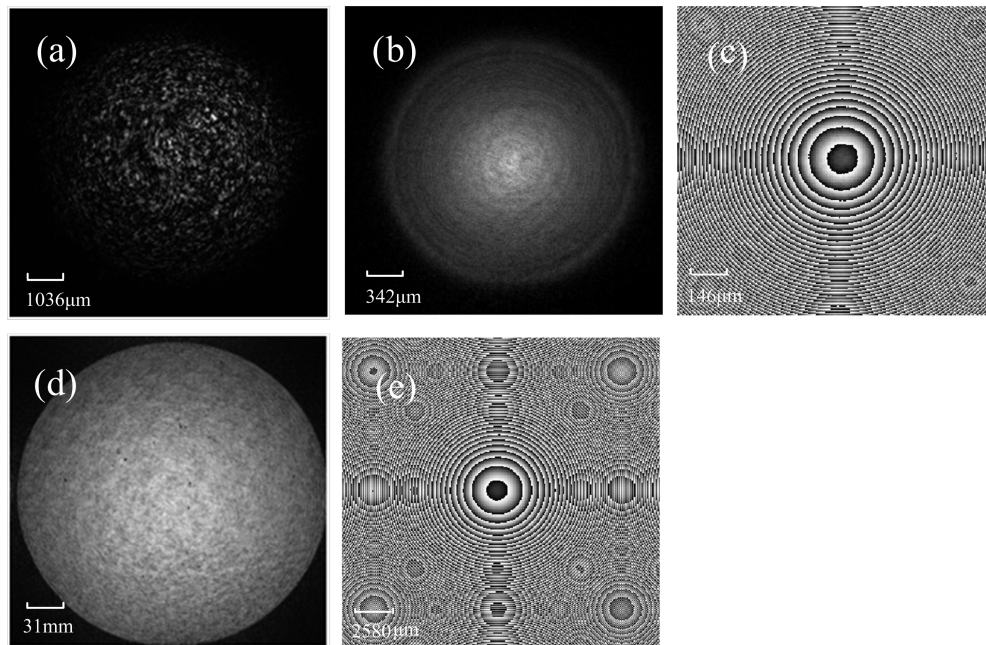

Fig. 4. The diffraction recorded and reconstructed results without CPP. (a)One of the diffraction patterns recorded by CCD, reconstructed modulus(b) and phase(c) distribution of illumination on scanning object, modulus(d) and phase (e)distribution of emergent light after the condenser lens.

The CPP is placed after the condenser lens and the above detecting and reconstruction procedures are repeated to measure the transmitting field $T(x, y)$. One of the recorded diffraction patterns is shown in Fig. 5(a), and the modulus and phase of the $P_1(x, y)$ are shown in Fig. 5(b). By propagating $P_1(x, y)$ to the back plane of the CPP we obtain the transmitting function $T(x, y)$, whose modulus and phase distributions are shown in Figs. 5(c) and 5(d) respectively. For the same reason as that explained above, only the central part of the phase is shown in Figs. 5(c) and 5(f) for the clarity.
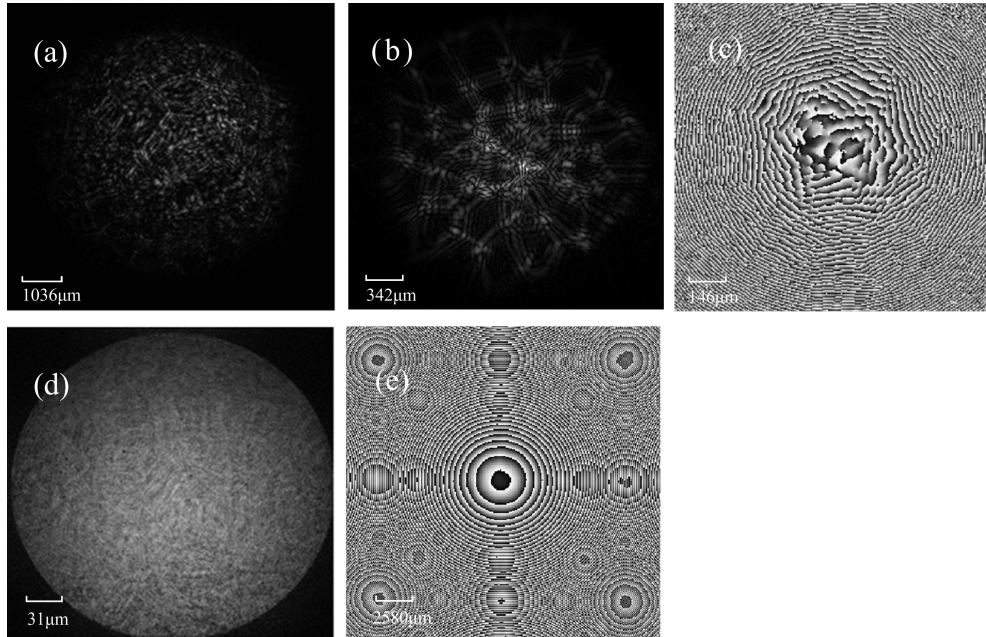

Fig. 5. The diffraction recorded and reconstructed results with CPP. (a)One of diffraction patterns recorded by CCD, reconstructed amplitude(b) and phase(c) distribution of illumination on scanning object, amplitude(d) and phase(e) distribution of emergent light after the condenser lens.

By calculating the phase of $U(x,y)T^*(x,y)$, the phase modulation of the CPP plate is obtained. Figure 6(a) is the wrapped phase of the measured phase modulation function, and Fig. 6(b) is the corresponding unwrapped phase distribution. We can quickly find out that the transmittance measurements made with ePIE are comparable to that of the design values of CPP [Fig. 3(b)]. For easy comparison, the values along the vertical lines and horizontal lines in Figs. 3(b) and 6(b) are plotted in Figs. 6(c) and 6(d), respectively, where the solid lines are the design value, and the dotted lines are the experimental value. We can find that the maximum difference between the measured and the designed value is only about 2.1rad, where the manufacturing accuracy is about one third of wavelength.

The experiment setup was calibrated by imaging a specially fabricated phase plate to find the exact distance between the CPP and the scanning object and to evaluate the measurement accuracy. The base of the calibrating plate is a smooth silicon plate with lots of tiny squares with a size of 148μm × 148μm etched on it. The depth of each etched square is about 316 ± 2 nm. Only when the distance used for the reconstruction is much accurate, the edge of these tiny squares can be clearly imaged, and at the calibrated distance the measurement accuracy is about 0.01λ. The details of the calibrating experiment are not demonstrated here. We can reasonably believe that the difference shown in Figs. 6(c) and 6(d) comes from the fabrication error of the CPP plate. We also want to point out that the spatial resolution of the measurement above is $du = \lambda z / N\Delta p$, where z is the distance between lens plane and the scanning object, N

is the number of the pixel of the CCD used, and Δp is the size of the each pixel. In the experiment $N\Delta p$ is 1.5 cm, the z is 1560mm, and the wavelength is 0.6328 μm. The spatial resolution determined is about 65μm, which is much higher than that of the Shack-Hartmann wavefront sensor.
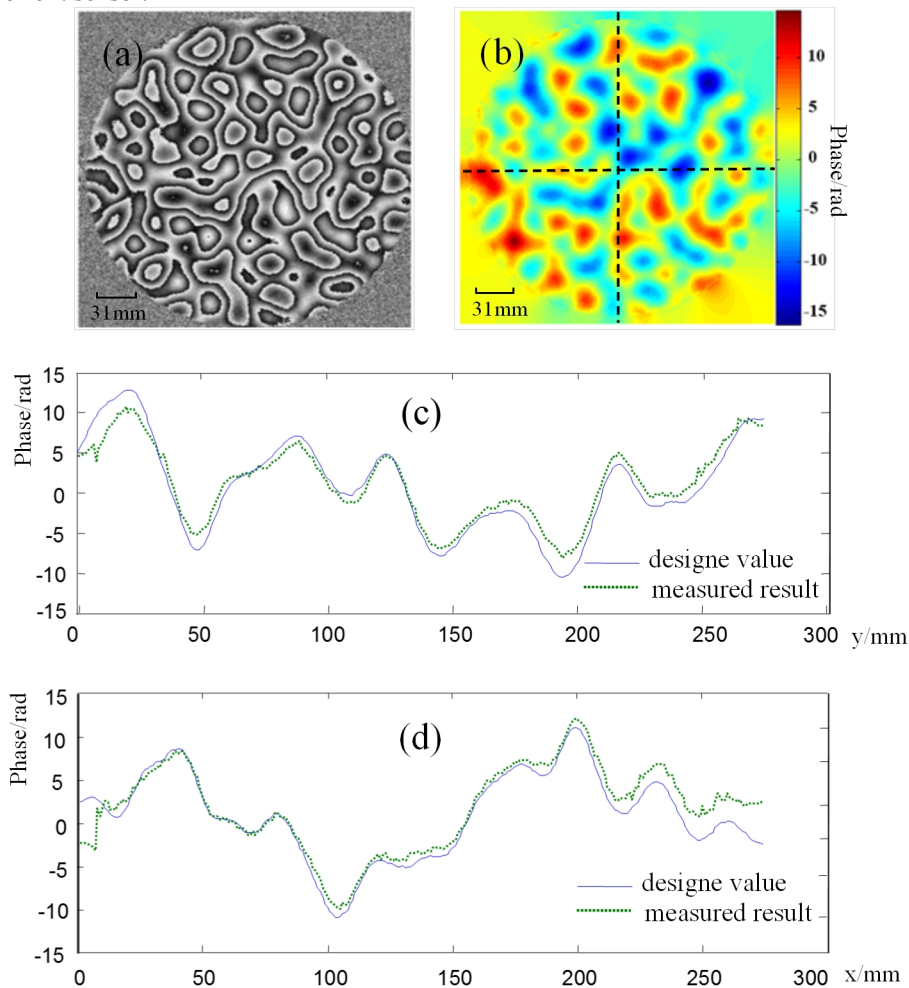

Fig. 6. (a) Wrapped phase of the measured modulation function, (b) wrapped phase of the measured modulation function, (c) the measured result and designed value alone the vertical lines of Figs. 3(b) and 6(b); (e) the measured result and designed value alone the horizontal lines of Figs. 3(b) and 6(b).

4. Conclusion

The ePIE algorithm is applied to measure the complex transmittance of large aperture optical element of ICF system. This technique can be extended to several large aperture elements, for which transmittance is not measureable using most of the commonly used techniques. Using a CPP plate as an example, which is a key optical element in high energy laser facility, the feasibility of the proposed method is demonstrated. To our knowledge, this is the first time that the ePIE technique is used for large optical element measurement.

Acknowledgments